

# Aero-Optical Investigation of Transonic Flow Features And Shock Dynamics on Hemisphere-On-Cylinder Turrets

Jacob Morrida<sup>1</sup>, Stanislav Gordeyev<sup>2</sup>, Nicholas De Lucca<sup>3</sup>, Eric Jumper<sup>4</sup>

*University of Notre Dame, Notre Dame, IN, 46545*

**Aero-optical environment around a hemisphere-on-cylinder turret with both flat- and conformal windows was studied experimentally in-flight using AAOL-T for a range of subsonic and transonic Mach numbers between 0.5 and 0.8. Above  $M = 0.6$ , the local shock appeared near the top of the turret, causing additional aero-optical distortions at side-looking angles. The instantaneous shock locations were extracted and analyzed. The mean shock location was found to be near  $\alpha = 80$  degrees for both window types at  $M = 0.7$  and  $0.8$ . For  $M = 0.8$ , the shock has a single frequency peak at  $St_D = 0.15$ , the same as for the unsteady separation line, indicating a possible lock-in mechanism between the shock and the separation region.**

## I. Introduction

As it is desirable to have airborne directed energy systems that are usable at cruise speeds in the high transonic flow regime with hemisphere-on-cylinder turrets, a detailed study of the transonic effects on turrets and their aero-optical implications is needed. The hemisphere-on-cylinder turret is geometry-of-choice for directed energy systems for maximizing the potential field-of-regard of a given system. Through the AAOL program, there have been many optical studies into subsonic and low-transonic flow regimes over various turret configurations [1,2,3]. Additionally, further work has been performed on cylindrical turrets to study shock dynamics and topology at transonic Mach numbers [4,5]. There has been limited work performed on turrets at transonic speeds outside of the AAOL program [6,7,8].

Flow over turrets is considered to enter the transonic flow regime for Mach numbers greater than 0.55 [6]. Above this critical Mach number, flow becomes locally supersonic on the turret. These locally supersonic flow regions can affect the various flow features on the turret. Figure 1 shows the flow features on a turret in the transonic regime. The most notable difference from a turret in subsonic flow is the presence of a shock on the turret. The exact location and behavior of this shock is dependent on the freestream Mach number [5]. This shock also can induce separation downstream of it, either causing premature wake formation or locally introducing additional optically-aberrating turbulence. Other than the presence of the shock, the subsonic flow features around the turret are still present in the transonic regime. A necklace vortex forms as the boundary layer rolls up near the base of the turret and extends downstream. Whether induced by the shock or the adverse pressure gradient on the downstream portion of the turret, separation occurs and forms a fully turbulent wake. The upstream portion of the turret exhibits little turbulence, as the accelerating flow remains attached and boundary layer is thin.

It is difficult to study realistic-size turrets at transonic speeds in tunnels, as it requires specially-designed and expensive to run tunnels with porous tunnel walls to eliminate the tunnel blockage effects. Furthermore, to perform aero-optical measurements in large tunnels is not a simple task. To overcome these difficulties, a successful AAOL program [1], designed to study aero-optical environment in flight, was recently transformed into AAOL-T program [9], using faster Falcon 10 planes, capable of flying up to  $M = 0.85$ , to specifically study transonic effects in flight.

---

<sup>1</sup> Graduate Student, Department of Mechanical and Aerospace Engineering, Hessert Laboratory for Aerospace Research, Notre Dame, IN 46556, AIAA Student Member.

<sup>2</sup> Research Associate Professor, Department of Mechanical and Aerospace Engineering, Hessert Laboratory for Aerospace Research, Notre Dame, IN 46556, AIAA Associate Fellow.

<sup>3</sup> Graduate Student, Department of Mechanical and Aerospace Engineering, Hessert Laboratory for Aerospace Research, Notre Dame, IN 46556, AIAA Student Member.

<sup>4</sup> Professor, Department of Mechanical and Aerospace Engineering, Hessert Laboratory for Aerospace Research, Notre Dame, IN 46556, AIAA Fellow.

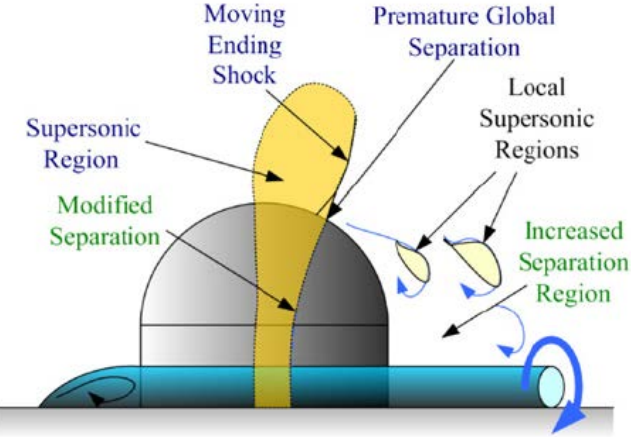


Figure 1. Transonic flow features on the turret. From [6].

This paper presents results of recent aero-optical flight measurements for the AAOL turret with different aperture geometries over a wide range of elevation and azimuthal angles for a range of Mach numbers between 0.5 and 0.8.

## II. Experimental Setup

Wavefront measurements were performed on the AAOL-T [9]. The AAOL turret is 1ft. in diameter with a 4 in. aperture, either flat or conformal one. The turret assembly features a fast steering mirror (FSM) to stabilize the beam on the optical bench. The AAOL-T program consists of two Falcon 10 aircraft flying in closed formation. The laser aircraft projects a diverging laser beam that overfills the aperture by a factor of 2 onto the turret of the laboratory aircraft. Aircraft separation is maintained at approximately 50 m while data is being acquired. Pictures of the turret and optical bench are shown in Figure 2 and Figure 3 shows a schematic of the optical setup in the laboratory aircraft.



Figure 2. The AAOL turret installed on AAOL-T, left and the instrumented optical bench, right.

Two separate flying campaigns were conducted to investigate aero-optics of the turret with different window geometries. During the first campaign, optical environment around the flat-window turret was investigated at the following Mach/altitudes: 0.5/15,000, 0.6/18,000, 0.7/26,000 and 0.8/26,000. During this campaign, wavefront measurements were performed using a high-speed Shack-Hartmann wavefront sensor. Similar to the data collection during AAOL program, two different acquisition modes were used for wavefronts: slewing maneuvers and fixed data. Slewing maneuvers involved the laser aircraft moving relative to the laboratory aircraft while wavefronts were continuously acquired; these maneuvers allow for rapid mapping of the optical environment around

the turret [2,3]. Fixed data involved the laser plane maintaining a fixed position with respect to the laboratory aircraft. These acquisitions were performed at a higher sampling rate, as the goal of fixed data acquisitions is to investigate specific flow phenomena with a better temporal resolution. Wavefronts were collected with the spatial resolution of 32x32 subapertures and sample rates of 25 kHz for 0.7 seconds for fixed points and 3 kHz for 10-30 seconds for slewing maneuvers. Simultaneous with the 2D wavefronts, the overall beam jitter was also measured using a position sensing device. The jitter was acquired along with the turret azimuthal/elevation angle and FSM position information at 25 kHz for 10s. Flight conditions were also recorded with the wavefront and jitter measurements. The aircraft separation was measured using a differential GPS system.

During the second campaign, the turret with both the flat- and the conformal windows was flown at the following Mach/altitudes: 0.5/15,000, 0.6/15,000, 0.6/16,000, 0.7/32,000, 0.7/35,000, 0.7/32,000 and 0.8/35,000 and optical data at both fixed points and slewing maneuvers were collected. During this campaign, wavefronts with collected with the better spatial resolution of 40x40 subapertures and sample rates of 30 kHz for fixed points and 2 kHz for slewing maneuvers. Simultaneous with the 2D wavefronts, the beam jitter was also measured using a position sensing device at 50 kHz for 30 seconds.

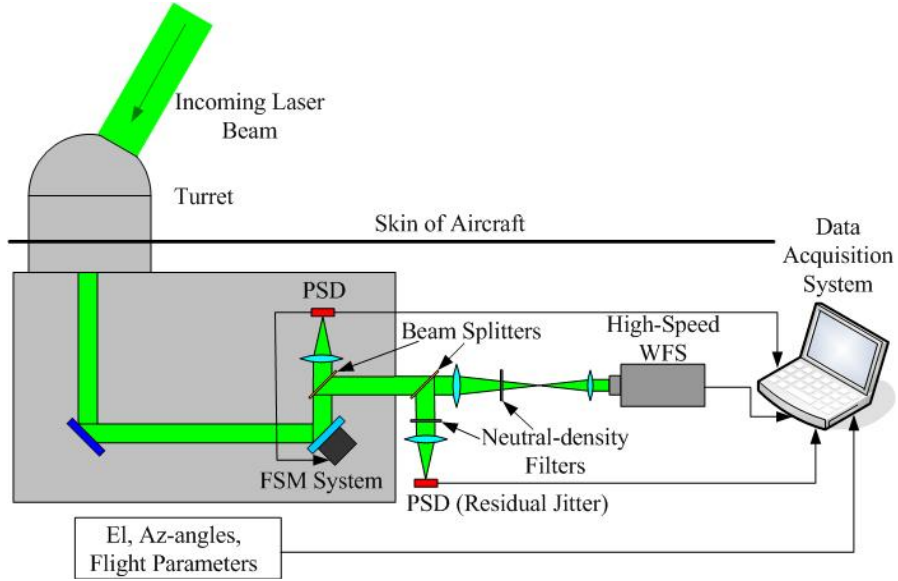


Figure 3. Schematic of the optical setup.

### III. Data Analysis

Reducing the Shack-Hartmann images gives the measured wavefronts,  $W$ , as a function of location on the aperture and time,  $W = W(\vec{x}, t)$ . Through least-squares plane fitting, any residual tip/tilt is removed from the wavefronts, and the steady lensing is removed by removing the mean of the wavefront at every subaperture. The optical path difference (OPD) is the conjugate of the wavefront,  $OPD(\vec{x}, t) = -W(\vec{x}, t)$ . To determine the variation of the OPD across the aperture, the spatial RMS is computed at every time step,

$$OPD_{RMS}(t) = \sqrt{\langle OPD(\vec{x}, t)^2 \rangle_{\vec{x}}} .$$

The time-average  $OPD_{RMS}$ , quantifies average amount of aberration present in the beam for a specific viewing direction. Similar to subsonic aero-optical studies, [2,3], the  $OPD_{RMS}$  is normalized by the flight conditions,

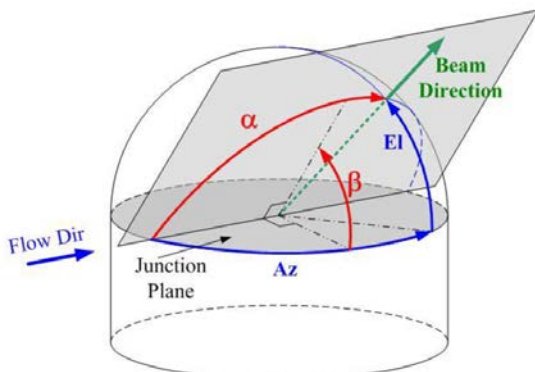


Figure 4. Relationship between azimuthal (Az) and elevation (El) angles to viewing angle ( $\alpha$ ) and modified elevation angle ( $\beta$ ). From [2].

$$OPD_{RMS,Norm} = OPD_{RMS} \left( \frac{\rho}{\rho_{SL}} M^2 D \right)$$

to compare the aero-optical performance of the turret across various Mach numbers. In this normalization,  $\rho$  is the freestream density,  $\rho_{SL}$  is the density at sea level,  $M$  is the Mach number and  $D$  is the turret diameter. This scaling has been previously shown to collapse subsonic data acquired in flight and in the tunnel [2].

The turret azimuthal (Az) and elevation (El) angles were recast into a coordinate system that is more useful from a fluid dynamics perspective. This system uses a viewing angle,  $\alpha$ , that determines how far downstream the turret is looking and the modified elevation angle,  $\beta$ , that quantifies how far the turret is looking away from the wall of the aircraft. The viewing angle is given by  $\alpha = \cos^{-1}(\cos(Az)\cos(El))$ , and the modified elevation angle is given by  $\beta = \tan^{-1}\left(\frac{\tan(El)}{\sin(Az)}\right)$ , as shown in Figure 4.

#### IV. Results

##### Flat-Window Turret

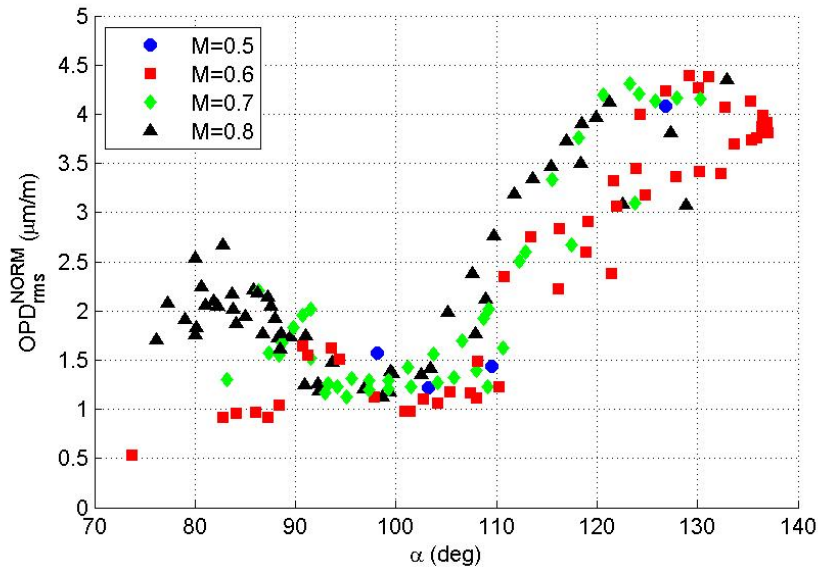


Figure 5. Normalized  $OPD_{RMS}$  versus viewing angle for  $M = 0.5-0.8$  for the flat-window turret.

Figure 5 shows the normalized  $OPD_{RMS}$  values for the flat-window turret as a function of Mach number and viewing angle. As  $M = 0.5$  was extensively studied during AAOL program, so only four points for  $M = 0.5$  were collected, mainly for comparison and repeatability purposes. For  $M = 0.6$ ,  $OPD_{RMS}$  values are fairly small for  $\alpha < 90^\circ$ , as the flow is attached over the flat-window aperture;  $OPD_{RMS}$  values are very similar to  $M = 0.5$  values, see [2]. Also, in [2] it was shown that at subsonic speeds over a range of viewing angles between  $90^\circ$  and  $100^\circ$ , a local separation bubble forms over the flat aperture, causing a local increase in  $OPD_{RMS}$  values. At  $M = 0.6$  the local shock on top of the turret is very weak to modify the otherwise subsonic flow over the turret, so a rather similar peak in  $OPD_{RMS}$  is present at  $M = 0.6$ ; the peak location is slightly shifted toward  $90^\circ$ . At  $\alpha = 110^\circ$  the flow separates, so for large viewing angles  $\alpha > 110^\circ$   $OPD_{RMS}$  continuously increase due to looking through the separated wake of the turret. Again, this behavior is very similar to  $OPD_{RMS}$  results at  $M = 0.5$ .

For a higher  $M = 0.7$ , the location of the local peak due to the separation bubble is around  $90^\circ$  and approximately unchanged from  $M = 0.6$ . The local peak is sharper, compared to  $M = 0.6$  case; inspection of wavefronts have revealed the presence of the shock approximately in the middle of the aperture. The flow separates around  $110^\circ$  as well, but the wake appears to be more optically-aberrating.

For  $M = 0.8$ , a stronger shock was found to be present over the flat aperture between viewing angles  $75^\circ$  and  $90^\circ$ , so the overall levels of  $OPD_{RMS}$  are significantly higher, compared values at the same angle range at lower Mach numbers. The shock was found to be unsteady and moving approximately in the middle of the aperture, see

spatial distributions of  $OPD_{RMS}$  for shock-induced wavefronts in Figure 6. The separation is also affected by the shock presence and appears to occur slightly upstream, at  $\alpha = 105^\circ$ , compared to  $M = 0.6$  and  $M = 0.7$ . There is no local peak that is indicative of a separation bubble for  $M = 0.8$ , indicating that the shock-induced separation prevents its formation.

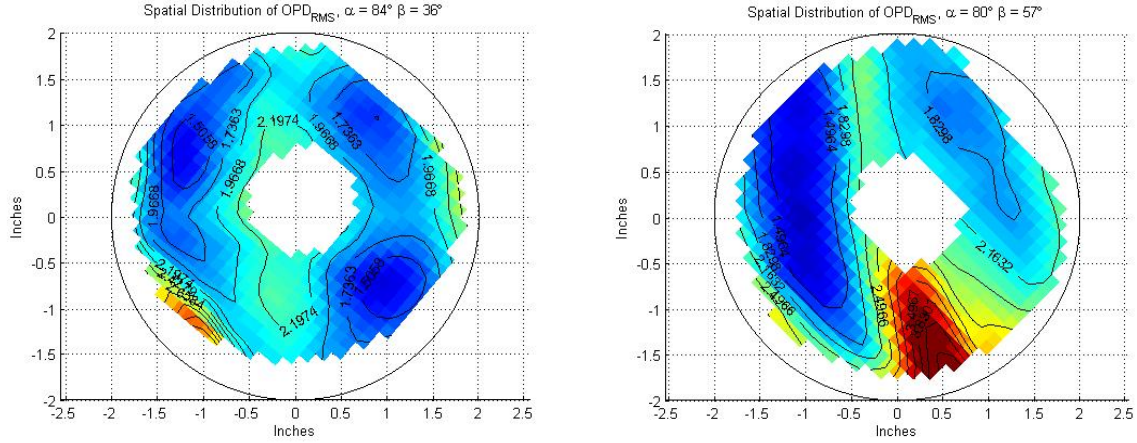


Figure 6. Spatial Distributions of OPD<sub>RMS</sub> for the flat-window aperture. Left: Az = 82° and El = 36° ( $\alpha=84^\circ$ ) M = 0.7. Right: Az = 72° and El = 56° ( $\alpha=80^\circ$ ) M = 0.8. Flow goes from left to right.

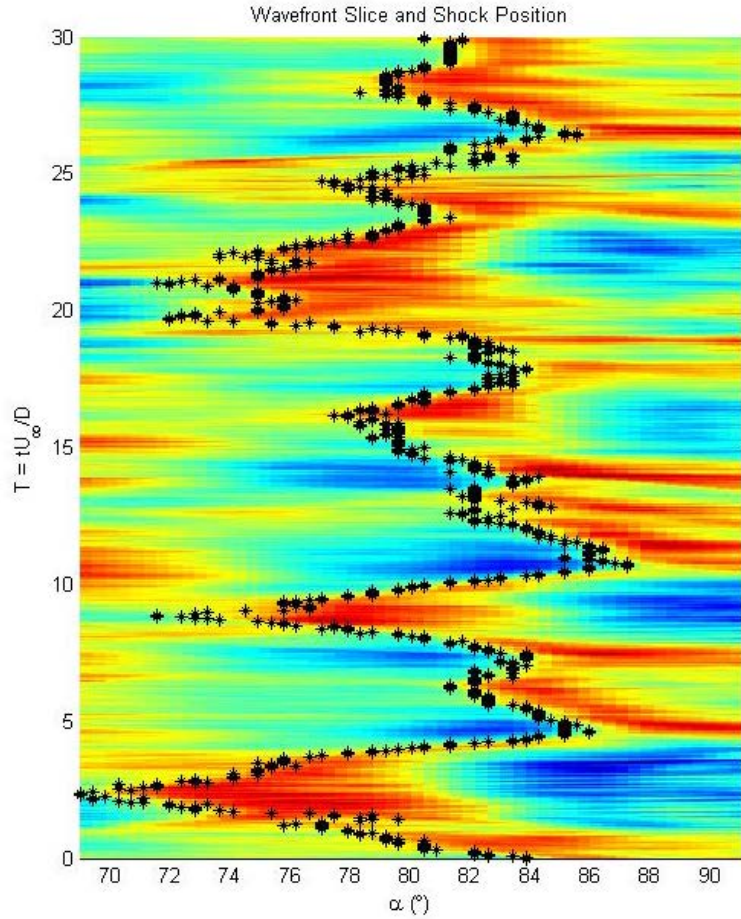


Figure 7: Spatial-temporal evolution of 1-D slice of wavefront for  $M = 0.8$  at  $\alpha = 80^\circ$ ,  $\beta = 43^\circ$ . Black circles indicate the approximate shock location.

The normalized spatial distributions of  $\text{OPD}_{\text{RMS}}$  are shown in Figure 6. Both the  $M = 0.7$  wavefronts, left and  $M = 0.8$  wavefronts, right show an increase in  $\text{OPD}_{\text{RMS}}$  in a narrow band near the center of the aperture due to the presence of the unsteady shock. This is the shock location for both cases. Because the shock location is near the center of the aperture, even though the viewing angle and Mach number are slightly different between the two cases, it is believed that the flat window has an “anchoring” effect on the shock in that it forces it to the center of the aperture, on average. One possible reason for this “anchoring” effect is that the separation bubble forms a fluidic curved surface over the aperture. The topology of the separation bubble is very sensitive to the flat-window position, as well as the flow environment. For  $M = 0.7$  the shock is formed over the curved fluidic surface, but the shock is fairly weak to modify it. The shock becomes much stronger at  $M = 0.8$ , essentially destroying the bubble. As it will be shown later in this paper in Figure 10, the resulted  $\text{OPD}_{\text{RMS}}$  for both the flat- and the conformal-window aperture are very similar at  $M = 0.8$ , confirming that the aperture geometry becomes a secondary factor, compared to the shock-induced effects.

Figure 7 shows a one-dimensional slice of wavefronts taken at  $M = 0.8$  for  $\alpha = 82^\circ$  and  $\beta = 43^\circ$ . The shock location was captured in  $\alpha$ - $\beta$  coordinates for given fixed  $\beta$ . The discontinuity of a shock causes a sharp change in the wavefront, so shock tracking was done by stepping along  $\alpha$  at the  $\beta$  of interest to find the location of maximum slope in the  $\text{OPD}_{\text{RMS}}$ ; a similar analysis was performed to study the shock dynamics on a 2D turret in the wind tunnel in [4,5]. The black filled circles show the location of maximum positive wavefront slope, which is presumed to be related to the instantaneous shock position. This maximum slope corresponds to the location of the shock. The shock moves between a relatively wide range of  $\alpha = 70^\circ$  and  $88^\circ$ ; this unsteady shock motion is as a cause of the increase in  $\text{OPD}_{\text{RMS}}$  observed in the  $M = 0.8$  data from Figure 5. The shock movement, although oscillatory, doesn’t appear to be periodic in nature and the shock does not “wander” off of the aperture.

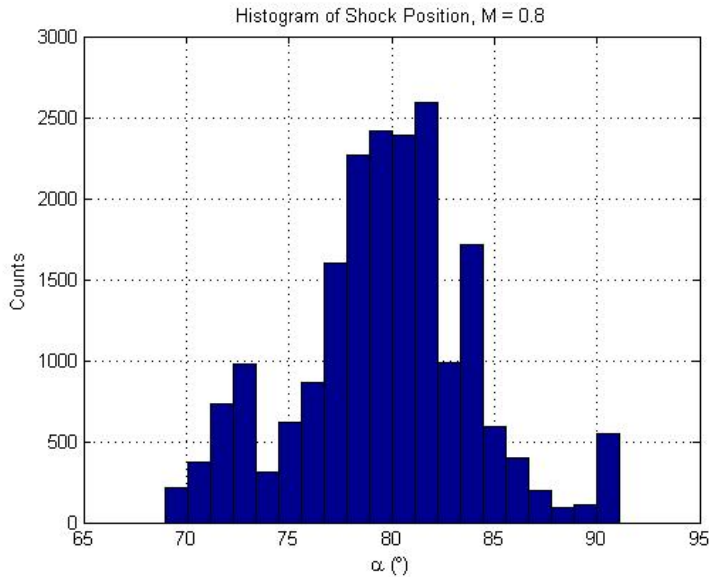


Figure 8: Histogram of the shock position for  $M = 0.8$  at  $\text{Az} = 72^\circ$ ,  $\text{El} = 56^\circ$ .

The histogram of the shock position for  $M = 0.8$  is shown in Figure 8. The shock is between  $71^\circ$  and  $87^\circ$  90% of the time, and the average location is at  $80^\circ$ . For  $M = 0.7$  (not shown), the shock moves approximately the same amount as for  $M = 0.8$ .

The spectra of the shock position for both  $M = 0.7$  and  $M = 0.8$  are shown in Figure 9. There isn’t much discernable difference between the frequency content of the shock movement for the two Mach numbers. Both exhibit a peak near  $\text{St} = 0.15$  and fall off after that. This peak has been associated with the movement of the separation line on a hemisphere on cylinder turret for subsonic [10] and transonic [11] flow regimes. As the separation bubble is sensitive to the global environment, which is primarily governed by the separated region downstream of the turret, this single peak in the shock spectra indicates that the shock dynamics is linked to the separation line dynamics.

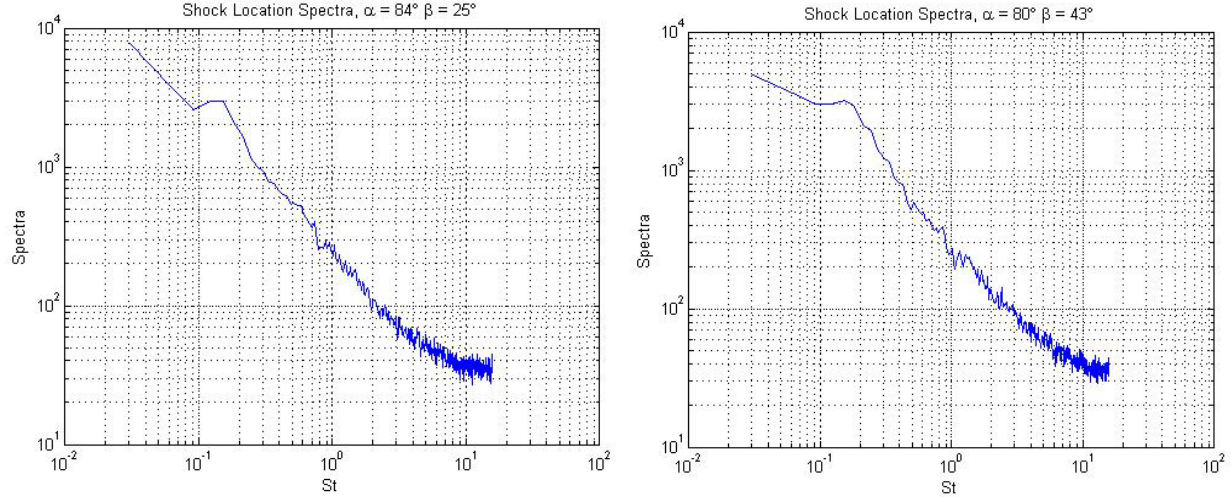


Figure 9: Shock location spectra for  $M = 0.7$ , left and  $M = 0.8$ , right.

#### Conformal-Window Turret

Figure 10 shows the normalized OPD<sub>RMS</sub> values for the conformal-window turret as a function of Mach number and viewing angle. As subsonic speeds of 0.5 and 0.6, the flow is subsonic everywhere around the turret. Unlike for the flat-window turret, shown in Figure 5, the flow stays attached over the aperture for side-looking angles 80-90 degrees with the low resulting OPDRms, as the conformal-window does not trip the flow around the aperture. For higher Mach numbers of 0.7 and 0.8 the unsteady shock appears over the aperture at the viewing angle of approximately 80 degrees, resulting in a local increase of OPDRms. Optical distortions at looking-back angles,  $\alpha > 100$  degrees, are due to the wake downstream of the turret and are similar both the flat- and conformal-window turrets.

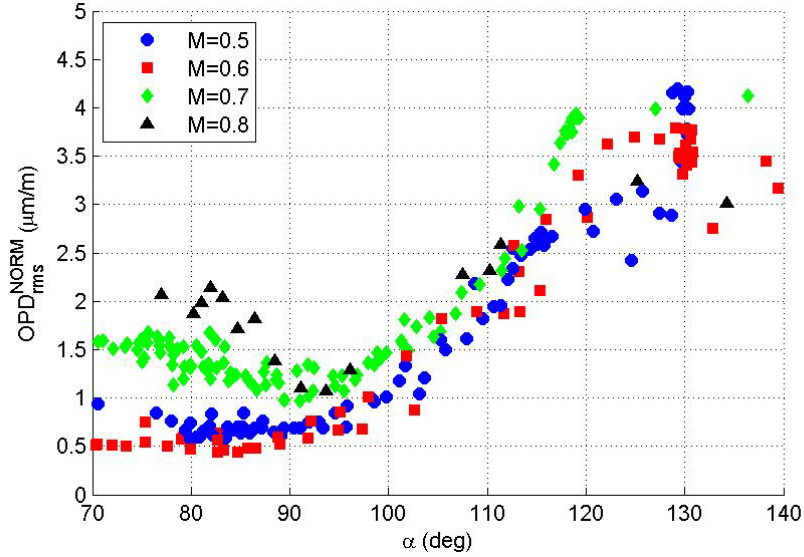


Figure 10. Normalized OPD<sub>RMS</sub> versus viewing angle for  $M = 0.5-0.8$  for the conformal-window turret.

To visualize the shock location on the turret, spatial variations of wavefronts at side-looking angles were projected on the turret. The shock creates additional localized distortions and it is visible as a line of the increased distortions, as shown in Figure 11. The average shock location is around  $\alpha = 80$  degrees and fairly independent of the elevation angle. The streamwise shock extent increases with the Mach number increase.

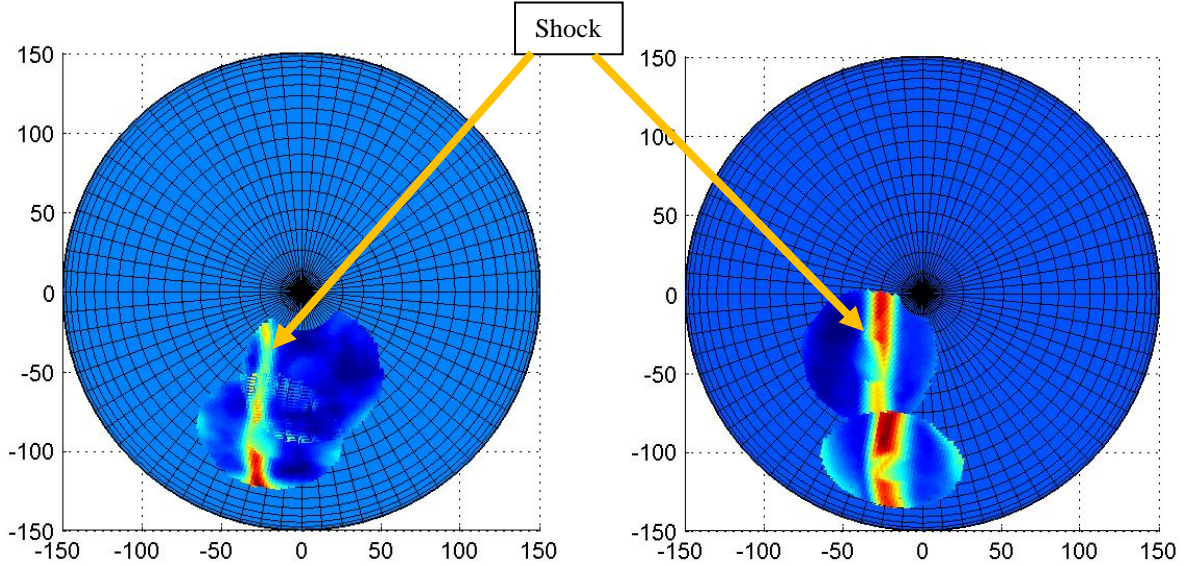


Figure 11. The top view of spatial variation of wavefronts for side-looking angles, indicating the shock location for  $M=0.7$  (left) and  $M=0.8$  (right). Flow goes from left to right.

To further study the temporal shock dynamics, spatial-temporal evolution 1-D slices of the wavefronts were extracted at different  $\beta$ -locations and Mach numbers and the instantaneous shock location was extracted, as it was described before. Figure 12 shows a one-dimensional slice of wavefronts for a conformal window turret taken at  $M = 0.7$  and  $M = 0.8$  with  $\beta = 60^\circ$  and  $\beta = 50^\circ$ , respectively. The black dots represent the shock location for each time step. The shock motion is not periodic for either case, although the shock for  $M = 0.8$  clearly has a single preferred frequency. Shocks are present consistently for each Mach number. The shock location for  $M = 0.7$  varies from  $79^\circ$  to  $88^\circ$ , while for  $M = 0.8$  it has a larger range of  $70^\circ$  to  $84^\circ$ . The  $M = 0.8$  case also has a larger non-dimensional time between peaks than the  $M = 0.7$  case, indicating a lower oscillation frequency content.

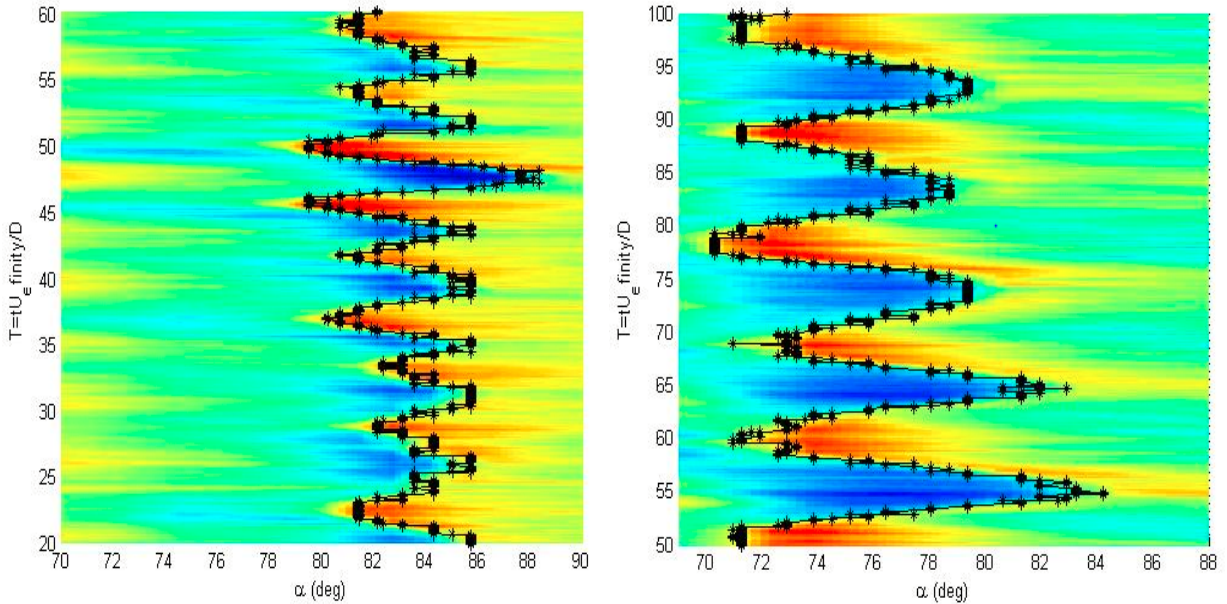


Figure 12: Spatial-temporal evolution of 1-D slice of wavefront data with  $M = 0.7$  (left) at  $\beta = 60^\circ$  and  $M = 0.8$  (right) at  $\beta = 50^\circ$ . Black circles indicate the approximate shock location.

Figure 13 depicts the mean shock locations at different  $\beta$ -angles with bars representing the range of  $\alpha$  where the shock is present 90% of the time. The mean shock location angle does not change significantly with changing  $\beta$ . For  $M = 0.8$  the shock tends to have a larger range, and for  $M = 0.7$  the mean shock location tends to be at slightly larger angles than the mean angular values for a given  $\beta$  for  $M = 0.8$ .

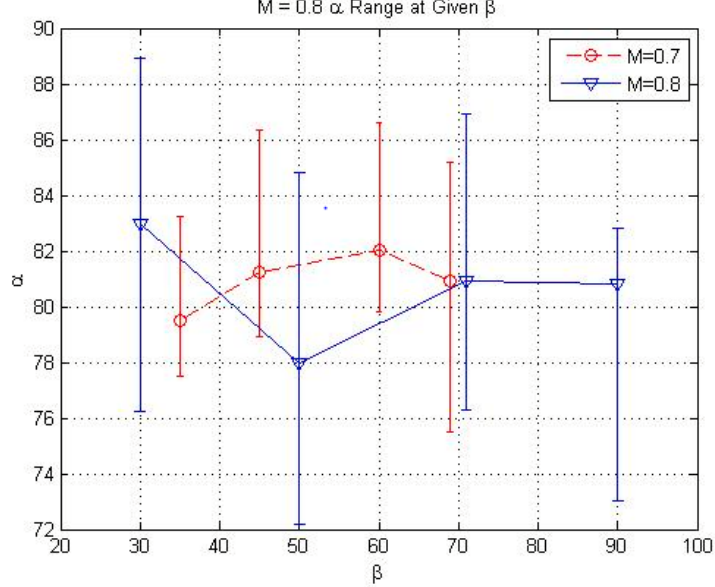


Figure 13: Shock mean locations and 90%-range for  $M = 0.7$  and  $M = 0.8$  for conformal-window turret.

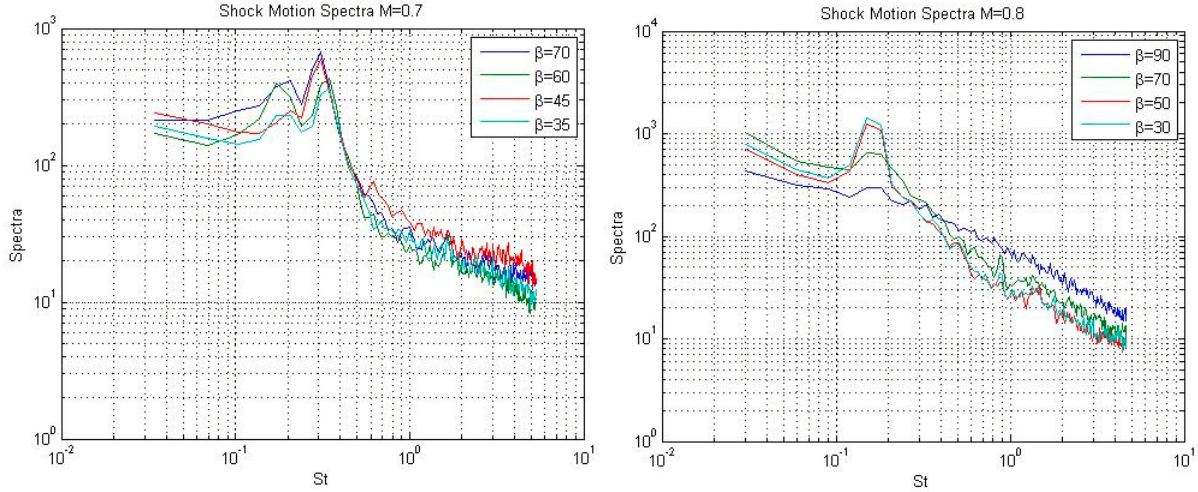


Figure 14: Conformal-Window shock location spectra for  $M = 0.7$ , left and  $M = 0.8$ , right.

The spectra of the shock position for a conformal window at  $M = 0.7$  and  $M = 0.8$  are shown in Figure 14. The most discernable difference between the two is that the  $M = 0.7$  case has peaks around  $St = 0.18$  and  $St = 0.3$ , while the  $M = 0.8$  case has only one peak near  $St = 0.15$ ; this lower-frequency dynamics was already observed in Figure 12. Results from pressure measurements in the wake [11] have showed similar peak locations for both  $M = 0.7$  and  $0.8$ . To understand a possible mechanism of this low-frequency dynamics, let us recall that a weaker, intermittent shock was observed on the AAOL at a lower  $M = 0.65$  [3] with a typical frequency of  $St \sim 0.5$ . Also,  $St = 0.15$  has been associated with the unsteady separation line motion over a wide range of subsonic [10] and transonic [11] Mach numbers. So, while at low transonic speeds the shock dynamics is independent of the separation region dynamics, at higher Mach number the shock becomes strong enough to force a premature separation, effectively coupling or locking-in the shock and the separation line dynamics. In [5] a strong coupling between shock location and strength with the location and size of the separated region was studied over cylindrical turrets and an acoustical

feedback was proposed as a possible mechanism for locking the dynamics of the shock and the shock-induced separation region.

## V. Conclusions

It is desirable to better understand the aero-optical environment around a hemisphere-on-cylinder turret for use in directed energy systems at transonic speeds. Using the AAOL-T, wavefront measurements were collected in-flight for a hemisphere-on-cylinder turret with conformal and flat windows in a transonic flow regime. Data was taken at different viewing angles, and the aero-optical environment was characterized by computing the OPD<sub>RMS</sub>. Shock dynamics were studied by using discontinuities in the OPD<sub>RMS</sub> to track their instantaneous locations.

The normalized OPD<sub>RMS</sub> was calculated for Mach numbers ranging from 0.5 – 0.8 on both the flat and conformal window turrets. It was found to have a local peak near  $\alpha = 80^\circ$  for the M = 0.7 and 0.8 cases. This peak was found to be due to the unsteady shock appearing in the optical wavefronts at this viewing angle. The shock location was found to almost independent of the modified elevation angle; the shock extent was increasing with the Mach number increasing.

The spectra of the shock motion was calculated for the M = 0.7 and 0.8 cases. For the flat-window aperture, spectral peaks occurred at St = 0.15 for both Mach numbers, which has been associated with the separation line motion. However, for the conformal window this peak only occurs at M = 0.8, while at M = 0.7 there are two peaks at St = 0.3 and 0.18. The decrease in the peak Strouhal number between M = 0.7 and 0.8 may be due to the interaction of the shock and the wake, as when the shock grows strong enough to cause a premature separation, it becomes locked into the same frequency as the separation line.

Future work will include collecting more data using the AAOL-T in order to acquire more information on the shock motion and to further study possible the proposed locking mechanism between the shock and wake. Additionally, wind tunnel tests will be performed to gather simultaneous pressure and wavefront measurements in order to track shock motion and its relation to the separated region motion.

## References

- [1] E Jumper, M Zenk, S Gordeyev, D Cavalieri and M. Whiteley, "Airborne Aero-Optics Laboratory", *Journal of Optical Engineering*, **52**(7), 071408, 2013.
- [2] C. Porter, S. Gordeyev, M. Zenk and E. Jumper, "Flight Measurements of the Aero-Optical Environment around a Flat-Windowed Turret", *AIAA Journal*, Vol. 51, No. 6, Jun. 2013, pp. 1394-1403.
- [3] N. De Lucca, S. Gordeyev and E.J. Jumper, "In-flight aero-optics of turrets", *Journal of Optical Engineering*, **52**(7), 071405, 2013.
- [4] R. Burns, S. Gordeyev, E. Jumper, S. Gogineni, M. Paul and D.J. Wittich, "Estimation of Aero-Optical Wavefronts Using Optical and Non-Optical Measurements", AIAA Paper 2014-0319.
- [5] A. Vorobiev, S. Gordeyev, E. Jumper, S. Gogineni, A. Marruffo and D.J. Wittich," Low-Dimensional Dynamics and Modeling of Shock-Separation Interaction over Turrets at Transonic Speeds", AIAA Paper 2014-2357, 2014.
- [6] S. Gordeyev and E. Jumper, "Fluid Dynamics and Aero-Optics of Turrets", *Progress in Aerospace Sciences*, **46**, (2010), pp. 388-400.
- [7] N. De Lucca, S. Gordeyev, E. Jumper and D.J. Wittich, "Aero-Optical Environment around Turrets at Forward-Viewing Angles", AIAA Paper 2013-0721, 2013.
- [8] R. Jelic, S. Sherer and R. Greendyke, "Simulation of Various Turret Configurations at Subsonic and Transonic Flight Conditions Using OVERFLOW", AIAA Paper 2012-464, 2012.
- [9] Jumper, E.J., Gordeyev, S., Cavalieri, D. and Rollins, P."Airborne Aero-Optics Laboratory - Transonic (AAOL-T)," to be presented at AIAA SciTech Forum 2015, 5 – 9 January, 2015.
- [10] S. Gordeyev, N. De Lucca, E. Jumper, K. Hird, T.J. Juliano, J.W. Gregory, J. Thordahl and D.J. Wittich, "Comparison of Unsteady Pressure Fields on Turrets with Different Surface Features using Pressure Sensitive Paint ", *Experiments in Fluids*, 55, p. 1661, 2014.
- [11] N. De Lucca, S. Gordeyev and E.J. Jumper, "Global Unsteady Pressure Fields Over Turrets In-Flight", to be presented at AIAA SciTech Forum 2015, 5 – 9 January, 2015.